

IMPROVING DEEP IMAGE MATTING VIA LOCAL SMOOTHNESS ASSUMPTION

Rui Wang¹, Jun Xie^{*2}, Jiacheng Han³, and Dezhen Qi⁴

¹Center for Applied Statistics and School of Statistics, Renmin University of China, Beijing 100872, China

²PCIE Lab, Lenovo Research, Beijing, China

³School of Optics and Photonics, Beijing Institute of Technology, Beijing, China

⁴Department of Physics, and Fujian Provincial Key Laboratory for Soft Functional Materials Research, Xiamen University, Xiamen 361005, China

wangrui.phd@ruc.edu.cn, xiejun@lenovo.com, 3220200419@bit.edu.cn, lucky7dz@stu.xmu.edu.cn

Abstract

Natural image matting is a fundamental and challenging computer vision task. Conventionally, the problem is formulated as an underconstrained problem. Since the problem is ill-posed, further assumptions on the data distribution are required to make the problem well-posed. For classical matting methods, a commonly adopted assumption is the local smoothness assumption on foreground and background colors. However, the use of such assumptions was not systematically considered for deep learning based matting methods. In this work, we consider two local smoothness assumptions which can help improving deep image matting models. Based on the local smoothness assumptions, we propose three techniques, i.e., training set refinement, color augmentation and backpropagating refinement, which can improve the performance of the deep image matting model significantly. We conduct experiments to examine the effectiveness of the proposed algorithm. The experimental results show that the proposed method has favorable performance compared with existing matting methods.

Key words: Image matting, backpropagating refinement, data augmentation.

^{*}Corresponding author

1 Introduction

Natural image matting is an important task in image editing. In this task, the natural image \mathcal{I} is assumed to be a convex combination of the foreground $\mathcal{F} \in \mathbb{R}^{h \times w \times 3}$ and the background $\mathcal{B} \in \mathbb{R}^{h \times w \times 3}$ weighted by $\alpha \in [0, 1]^{h \times w}$, the opacity of the foreground. Formally, the color at $i \in \{1, \dots, h\} \times \{1, \dots, w\}$ satisfies the compositing equation

$$\mathcal{I}_i^c = \alpha_i \mathcal{F}_i^c + (1 - \alpha_i) \mathcal{B}_i^c, \quad c = 1, 2, 3. \quad (1)$$

Given an input image \mathcal{I} , the goal of natural image matting is to estimate α . Note that there are 3 equations with 7 unknowns at each pixel, which results in the nonidentifiability of \mathcal{F} , \mathcal{B} and α . Specifically, suppose that the triplet $(\mathcal{F}, \mathcal{B}, \alpha)$ satisfies (1). Then for any $\mathcal{Q} \in \mathbb{R}^{h \times w}$ satisfying $0 \leq \mathcal{Q}_i \leq \frac{1}{\alpha_i}$, the triplet $((\mathcal{B}_i^c + (\mathcal{F}_i^c - \mathcal{B}_i^c)/\mathcal{Q}_i), \mathcal{B}, (\mathcal{Q}_i \alpha_i))$ also satisfies (1). Thus, without further assumption, the natural image matting problem is ill-posed.

To regulate the problem, natural image matting is often aided by human. In a typical human-aided process, the user provides a trimap $\mathcal{T} \in \{0, 0.5, 1\}^{h \times w}$ indicating the purely foreground region $\{i : \mathcal{T}_i = 1\}$, the purely background region $\{i : \mathcal{T}_i = 0\}$, and the unknown region $\{i : \mathcal{T}_i = 0.5\}$. It is guaranteed that if $\mathcal{T}_i = 1$ then $\alpha_i = 1$ and if $\mathcal{T}_i = 0$ then $\alpha_i = 0$. Given a trimap \mathcal{T} , one only needs to estimate α in the unknown region. However, the compositing equation

(1) is still ill-posed in the unknown region. In principle, further assumptions are still required to make the problem well-posed.

For traditional natural image matting methods, local smoothness assumptions on \mathcal{F} , \mathcal{B} or α are commonly used. In the seminal work of [1], the authors proposed the color line model based on the assumption that \mathcal{F} and \mathcal{B} are approximately constant locally. There are also methods which utilize smoothness assumptions on α ; see [2] and the references therein. For traditional methods, a main goal of imposing local smoothness assumptions is to formulate tractable models. Consequently, these assumptions may be overly strong.

Thanks to the large training data released by Xu *et al.* [3] and the advent of convolutional neural networks, deep learning based matting methods have achieved significantly better performances than traditional methods [3, 4, 5, 6, 7, 8]. For deep learning methods, one does not need to formulate an explicit model of colors as in traditional methods. However, this does not mean that the local smoothness assumptions are unimportant for deep image matting. Rather, the deep neural networks may learn the implicit local smoothness assumptions during the training phase. Intuitively, deep learning methods may be improved if they are guided by local smoothness assumptions. Unfortunately, to our best knowledge, no existing deep learning method utilizes the local smoothness assumptions explicitly.

In this paper, we explore the use of local smoothness assumption in deep image matting. We consider two seemingly trivial assumptions that should be satisfied by natural images. Surprisingly, even these simple assumptions can be violated by modern deep image matting methods. We propose three techniques to guide deep image matting methods based on the local smoothness assumptions. The proposed three techniques work in the different stage of deep learning methods. We observe that the foreground images in the widely used Adobe Image Matting (AIM) dataset [3] violates our first assumption. Hence our first technique is a training set refinement method which improves the AIM training set. The second technique is a color augmentation method which functions in the training phase. This technique can further improve

the local smoothness property of the training data. The third technique is a backpropagating refinement method which functions in the inference phase. It enforces the output of the deep network to satisfy our second assumption. We conduct experiments to evaluate the effectiveness of the proposed techniques. In summary, the contributions of the present paper are as follows:

- This work is the first one to systematically explore the local smoothness assumptions in deep image matting.
- We propose three novel techniques to significantly improve the performance of deep image matting models. In particular, this work is the first deep image matting method which considers backpropagating refinement during the inference phase.
- Based on the proposed techniques, we present a simple deep image matting model which achieves the state-of-the-art performance on the testing set of [3] among all methods trained solely on AIM dataset.

2 Related works

A class of classical matting methods are based on pixel sampling. These methods sample colors from the known foreground region and known background regions, and use them to estimate α_i in the unknown region. Matting methods based on pixel sampling include [9, 10, 11, 12, 13, 14].

Another traditional approach to the natural image matting problem is based on affinities between pixels. These methods make use of pixel similarities to propagate the alpha values from the region of $\{i : \mathcal{T}_i = 0\} \cup \{i : \mathcal{T}_i = 1\}$ to the region of $\{i : \mathcal{T}_i = 0.5\}$. Poisson matting method [15] impose a model of the gradient of \mathcal{I} and α and use Poisson equations to characterize the affinities between pixels. [1] proposed a color line model based on local smoothness assumptions and obtain a closed-form matting method. [16] proposed a KNN matting method which incorporates nonlocal information. [17] conceptualized the affinities as information flows and designed

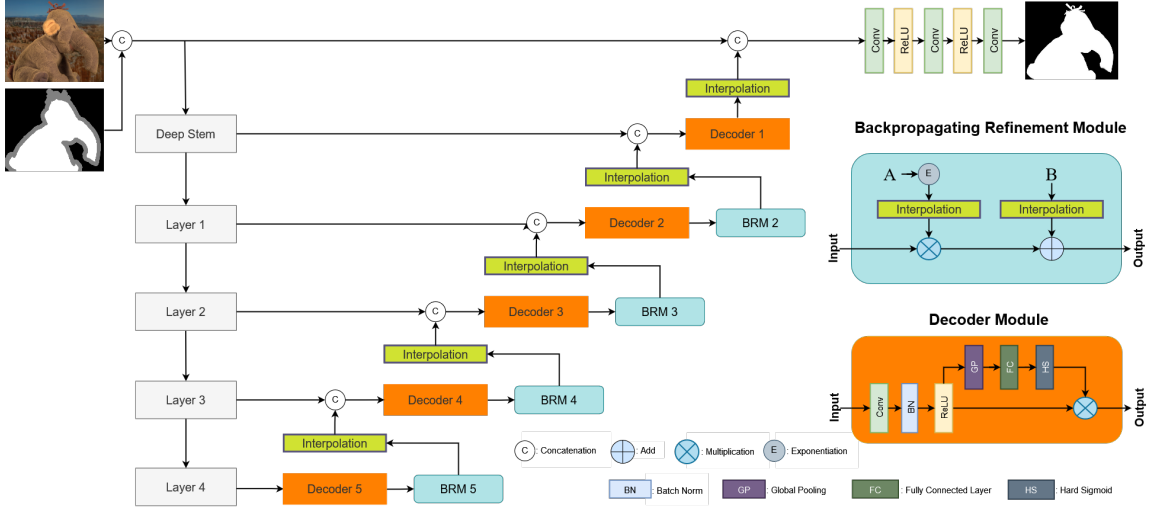


Figure 1: Proposed network architecture.

several information flows to control the way of propagation.

The deep learning method was introduced to the matting problem by [18]. [3] released a large scale matting dataset which greatly facilitated the subsequent deep learning methods for natural image matting. [19] explored adversarial training in deep image matting. [20] designed an upsampling module for matting. [5] proposed a deep learning based sampling method. [21] disentangled the matting problem to trimap adaptation and alpha estimation. [4] proposed a nonlocal module to capture long-range contexts. [6] proposed a network which can simultaneously estimate \mathcal{F} , \mathcal{B} and α . [7] proposed a deep learning method to deal with images with extremely large size. [8] proposed a network which incorporates semantic classification.

Besides the deep learning methods mentioned above, there are also some deep learning methods which do not need an input trimap; see, e.g., [22, 23].

3 A Baseline Deep Image Matting Model

In this section, we introduce a simple deep neural network for natural image matting which serves as the baseline model.

Network architecture. Our network, as illustrated in Figure 1, has a standard encoder-decoder architecture. The encoder is ResNet-50-D [24] which is a variant of ResNet-50 [25]. The input to the encoder is the concatenation of the image and trimap, which has 4-channels. The input image is downsampled 5 times in the encoder. For the baseline model, the backpropagating refinement module is simply the identity operator. For the decoder module, we adopt a block which is similar to the SE block [26] to fuse the global information of the image. This module is adapted from VoVNet [27]. Compared with the SE block, the module we use only involves one convolution and uses a hard sigmoid function to give a fast approximation to the sigmoid.

Loss function. Xu *et al.* [3] considered the loss function

$$L(\hat{\alpha}, \alpha) = \frac{1}{\text{Card}(\{i : \mathcal{T}_i = 0.5\})} \sum_{\{i : \mathcal{T}_i = 0.5\}} \sqrt{(\hat{\alpha}_i - \alpha_i)^2 + \epsilon^2}.$$

To measure the difference of $\hat{\alpha}$ and α at different scales, we apply the above loss function at various scales of $(\hat{\alpha}, \alpha)$ and use their weighted sum as the final loss function. Specifically, the loss function we use is $\sum_{\ell=0}^4 2^{-\ell} L(\mathcal{P}^\ell(\hat{\alpha}), \mathcal{P}^\ell(\alpha))$, where \mathcal{P}^ℓ denotes the average pooling operator with kernel size $2^\ell \times 2^\ell$ and stride 2^ℓ .

4 Utilizing Local Smoothness Assumptions

For a position i , let $\partial\{i\}$ denote the set of 4 surrounding positions of i . For a region R , let ∂R denote the boundary of R . Formally, $i \in \partial R$ if and only if $(\{i\} \cup \partial\{i\}) \cap R \neq \emptyset$ and $(\{i\} \cup \partial\{i\}) \cap R^c \neq \emptyset$. We consider the following two modest local smoothness assumptions.

Assumption 1. \mathcal{F} is locally constant at the positions

$$\{i : \alpha_i = 0\} \cup \partial\{i : \alpha_i = 0\}.$$

Assumption 2. α is locally constant at the positions

$$\partial\{i : \mathcal{T}_i = 1\} \cup \partial\{i : \mathcal{T}_i = 0\}.$$

Assumptions 1 and 2 impose conditions on \mathcal{F} and α , respectively. We do not impose any condition on \mathcal{B} . In fact, the background \mathcal{B} is often an unconstrained natural image in practice. Assumptions 1 and 2 are fairly weak, and we can expect them to hold for general natural images.

To justify Assumption 1, we note that according to the compositing equation (1), the value of \mathcal{F} in the region $\{i : \alpha_i = 0\}$ does not affect the color of \mathcal{I} , and hence can be arbitrarily defined. However, the foreground colors in the region $\{i : \alpha_i = 0\}$ do have impact on the training process of deep image matting model. In fact, some commonly adopted data augmentation techniques, e.g., image resize and image rotation, rely on interpolation techniques. When interpolation techniques are applied to \mathcal{F} , the foreground colors in the region $\{i : \alpha_i = 0\}$ may contaminate the colors in the region $\{i : \alpha_i > 0\}$. This phenomenon was observed by [6]. The problem of color contamination is eased by Assumption 1. In fact, under Assumption 1, for a position i in $\{i : \alpha_i > 0\}$,

the sampling points of the interpolation method has similar foreground colors as i and hence will not contaminate the color of i .

To justify Assumption 2, we note that the trimap provided by users are often coarse. Since the trimap must be precise, the users may tend to be conservative and do not label pixels near the region $\{i : 0 < \alpha_i < 1\}$ to be foreground or background. As a result, the pixels near the region $\{i : \mathcal{T}_i = 1\}$ are very likely to have opacity exactly 1, and the pixels near the region $\{i : \mathcal{T}_i = 0\}$ are very likely to have opacity exactly 0. Further, for the open matting datasets of [28] and [3], the trimaps are based on dilations of the region $\{i : 0 < \alpha_i < 1\}$. For these datasets, Assumption 2 holds strictly. In summary, Assumption 2 is a weak and reasonable assumption.

Below we propose three techniques based on Assumptions 1 and 2 to improve deep image matting.

4.1 Refining Training Set

We have noted that the violation of Assumption 1 may result in the color contamination. To ease this problem, Forte and Pitié [6] used the closed-form foreground estimation method of [1] to re-estimate the foregrounds in AIM dataset. However, The method of [1] is not designed to meet Assumption 1. We shall see that their method has suboptimal performance compared with the proposed re-estimation method.

Now we propose a new method to re-estimate the foregrounds in AIM training dataset. Formally, the re-estimation problem is as follow: given an initial foreground \mathcal{F} and α , the goal is to output a re-estimated $\hat{\mathcal{F}}$ such that $\hat{\mathcal{F}}$ has similar behavior as \mathcal{F} when used to compose an image and that $\hat{\mathcal{F}}$ satisfies Assumption 1. To meet these two requirements, we would like to minimize the following cost function:

$$C(\hat{\mathcal{F}}, \mathcal{F}) = \frac{1}{2} \sum_{i \in \{1, \dots, h\} \times \{1, \dots, w\}} \sum_{c=1}^3 \left\{ \alpha_i^2 (\hat{\mathcal{F}}_i^c - \mathcal{F}_i^c)^2 + \kappa (1 - \alpha_i)^2 \sum_{j \in \partial\{i\}} (\hat{\mathcal{F}}_i^c - \hat{\mathcal{F}}_j^c)^2 \right\},$$

where $\kappa > 0$ is a hyperparameter. The cost $\alpha_i^2 (\hat{\mathcal{F}}_i^c - \mathcal{F}_i^c)^2$ ensures $\hat{\mathcal{F}}_i^c$ is close to \mathcal{F}_i^c when α_i is large. On

the other hand, the cost $(1 - \alpha_i)^2 \sum_{j \in \partial\{i\}} (\hat{\mathcal{F}}_j^c - \hat{\mathcal{F}}_i^c)^2$ ensures that $\hat{\mathcal{F}}_i^c$ is locally smooth when α_i is small, which conforms Assumption 1. The derivative of $C(\hat{\mathcal{F}}, \mathcal{F})$ is

$$\begin{aligned} \frac{\partial C(\hat{\mathcal{F}}, \mathcal{F})}{\partial \hat{\mathcal{F}}_i^c} = & \left(\alpha_i^2 + 4\kappa(1 - \alpha_i)^2 + \kappa \sum_{j \in \partial\{i\}} (1 - \alpha_j)^2 \right) \hat{\mathcal{F}}_i^c \\ & - \alpha_i^2 \mathcal{F}_i^c - \kappa \sum_{j \in \partial\{i\}} ((1 - \alpha_i)^2 + (1 - \alpha_j)^2) \hat{\mathcal{F}}_j^c. \end{aligned}$$

Setting the derivative $\partial C(\hat{\mathcal{F}}, \mathcal{F})/\partial \hat{\mathcal{F}}_i^c$ to zero yields

$$\hat{\mathcal{F}}_i^c = \frac{\alpha_i \tilde{\mathcal{I}}_i^c + \kappa \sum_{j \in \partial\{i\}} ((1 - \alpha_i)^2 + (1 - \alpha_j)^2) \hat{\mathcal{F}}_j^c}{\alpha_i^2 + 4\kappa(1 - \alpha_i)^2 + \kappa \sum_{j \in \partial\{i\}} (1 - \alpha_j)^2},$$

where $\tilde{\mathcal{I}}_i^c := \alpha_i \mathcal{F}_i^c$. According to the above formula, a simple iteration algorithm can be obtained immediately, as summarized in Algorithm 1.

Algorithm 1: Simple Foreground Refining Algorithm

Function SimpleRefine($\tilde{\mathcal{I}}, \alpha, \mathcal{F}_{\text{init}}, \kappa, T$):
 $w \leftarrow \text{width of } \mathcal{F}; h \leftarrow \text{height of } \mathcal{F}$
 $\hat{\mathcal{F}}(0) \leftarrow \mathcal{F}_{\text{init}}$
for $t \leftarrow 0$ **to** $T - 1$ **do**
 for $i \leftarrow 1$ **to** wh **do**
 for $c \leftarrow 1$ **to** 3 **do**
 $\hat{\mathcal{F}}_i^c(t+1) \leftarrow \frac{\alpha_i \tilde{\mathcal{I}}_i^c + \kappa \sum_{j \in \partial\{i\}} ((1 - \alpha_i)^2 + (1 - \alpha_j)^2) \hat{\mathcal{F}}_j^c(t)}{\alpha_i^2 + 4\kappa(1 - \alpha_i)^2 + \kappa \sum_{j \in \partial\{i\}} (1 - \alpha_j)^2}$
 return $\hat{\mathcal{F}}(T)$

In each iteration of Algorithm 1, the color in a pixel is only affected by its surrounding 4 pixels. Due to the slow speed of foreground color propagation, Algorithm 1 may have an extremely large mixing time. Motivated by the fast multi-level foreground estimation method [29], we propose a multi-level refining procedure which first performs Algorithm 1 on the downsampled image, and gradually increases the image size to the original size. We summarize the multi-level algorithm in Algorithm 2. In practice, the pa-

Algorithm 2: Multi-Scale Foreground Refining Algorihtm

Input: Foreground \mathcal{F} ; Opacity α ; Scale number S ; Hyperparameter κ ; Iteration number T ;
 $w \leftarrow \text{width of } \mathcal{F}; h \leftarrow \text{height of } \mathcal{F}$
 $\mathcal{F}_{\text{init}} \leftarrow \mathcal{F}; \tilde{\mathcal{I}} \leftarrow \alpha \mathcal{F}$
for $s \leftarrow S - 1$ **to** 0 **do**
 $\tilde{\mathcal{I}}_s \leftarrow \text{Resize}(\tilde{\mathcal{I}}, 2^{-s}w, 2^{-s}h)$
 $\alpha_s \leftarrow \text{Resize}(\alpha, 2^{-s}w, 2^{-s}h)$
 $\mathcal{F}_{\text{init}} \leftarrow \text{Resize}(\mathcal{F}_{\text{init}}, 2^{-s}w, 2^{-s}h)$
 $\mathcal{F}_{\text{init}} \leftarrow \text{SimpleRefine}(\tilde{\mathcal{I}}_s, \alpha_s, \mathcal{F}_{\text{init}}, \kappa, 2^s T)$
return $\mathcal{F}_{\text{init}}$

rameters in Algorithm 2 are $S = 6$, $\kappa = 1$, $T = 20$ and the resize operator is the bilinear interpolation.

In Fig. 2, we illustrate the effect of re-estimation of \mathcal{F} on an image in the training set of AIM [3]. It can be seen that, before re-estimation, the foreground has large variation when α_i is near 0, which violates Assumption 1. After we re-estimate the foreground using the proposed algorithm, the foreground is much smoother when α_i is near 0. Also, the foreground should be continuous in the region $\{i : \alpha_i = 0\}$.

4.2 Color Augmentation

In this section, we propose a simple color augmentation method to augment the training data. Given a foreground \mathcal{F} , We randomly generate an image $\tilde{\mathcal{I}}$ with a constant color u , i.e., $\tilde{\mathcal{I}}_i = u$ for all i , and a random number $w \in [0, 1]$. The augmented foreground is defined as $\tilde{\mathcal{F}} = w\mathcal{F} + (1 - w)\tilde{\mathcal{I}}$. To see why this simple augmentation method can work, we note that the gradient of $\tilde{\mathcal{F}}$ is $\nabla \tilde{\mathcal{F}} = w\nabla \mathcal{F}$. Since $w < 1$, the augmented image $\tilde{\mathcal{F}}$ is smoother than \mathcal{F} . Consequently, the augmented image is more consistent with Assumption 1.

4.3 Backpropagating Refinement

Now we consider the use of Assumption 2 which basically assumes that the predicted opacity $\hat{\alpha}$ should

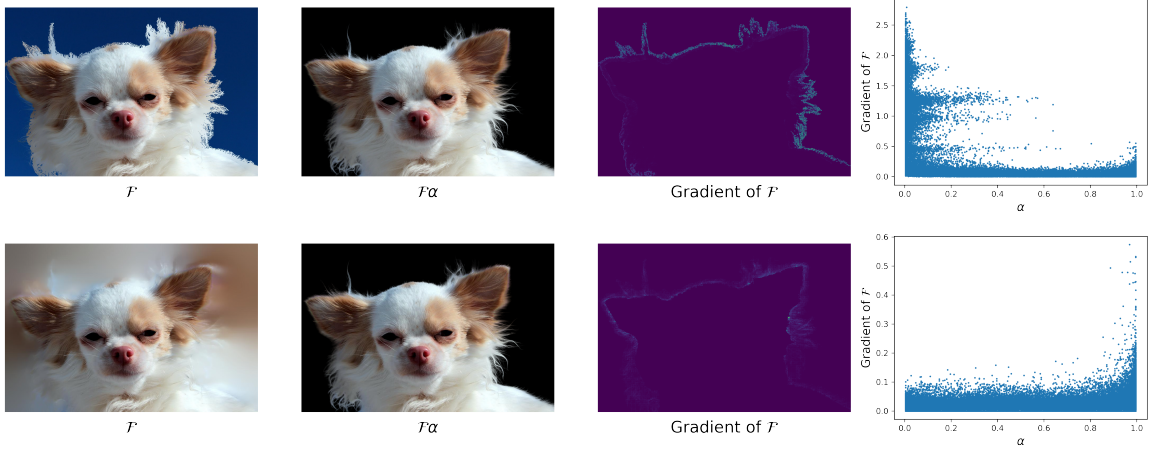


Figure 2: Illustration of the effect of re-estimation of \mathcal{F} . Figures in the first row are for the original \mathcal{F} . Figures in the second row are for the re-estimated \mathcal{F} . The first column is the image \mathcal{F} . The second column is the image $\mathcal{F}\alpha$. The third column is the gradient of \mathcal{F} . The Fourth column is the plot of the gradient of \mathcal{F} versus α within the region $\{i : 0 < \alpha_i < 1\}$.

take value 1 on $\partial\{i : \mathcal{T}_i = 1\}$ and take value 0 on $\partial\{i : \mathcal{T}_i = 0\}$. Intuitively, this assumption should be automatically satisfied for reasonable matting methods. Surprisingly, as illustrated in the first row of Fig. 3, even for deep image matting models whose performance is close to the current state-of-the-art, the output of the network can violate Assumption 2. It shows that deep learning methods may not automatically guarantee that the known pixels annotated by the trimap has the correct result. In fact, similar phenomenon was previously observed in the field of interactive image segmentation [30, 31].

There are two possible causes of this phenomenon. First, in the training phase of most existing methods, the trimap is obtained by dilating the regions $\{i : \alpha_i > 0\}$ and $\{i : \alpha_i < 1\}$. However, the trimap so obtained can not fully mimick the input trimap generated by users, resulting in poor performance when the trimap is provided by users. Second, convolutional neural networks may not make good use of the sparse region of trimap. Specifically, suppose R is a connected component of the the region $\{i : \mathcal{T}_i = 1\}$. If the area of R is small, then the information provided by R may not be well used by the deep image

matting model.

Given a testing image \mathcal{I} and its trimap \mathcal{T} , if the output of the deep image matting model does not satisfy Assumption 2, we would like to regulate the output such that Assumption 2 is satisfied. To achieve this, the idea is to use a backpropagating procedure to refine the result during the inference process. The use of backpropagating refinement in the inference phase has achieved great success for the interactive segmentation task [30, 31]. To the best of our knowledge, the use of backpropagating refinement in deep image matting has never been explored before.

Our backpropagating refinement method works as follows. For $2 \leq \ell \leq 5$, the output of Decoder ℓ is processed by a Backpropagating Refinement Module (BRM) whose architecture is illustrated in Fig. 1. For BRM ℓ , $2 \leq \ell \leq 5$, there are two trainable parameters \mathbf{A} and \mathbf{B} which are both tensors with dimension $(2^{8-\ell}, 2^{8-\ell}, C)$ where C is the channel number of the input of BRM. The output of BRM is $\exp(\mathcal{I}(\mathbf{A})) \cdot \text{Input} + \mathcal{I}(\mathbf{B})$, where \mathcal{I} is the interpolation operator such that $\mathcal{I}(\mathbf{A})$ and $\mathcal{I}(\mathbf{B})$ have the same dimension as the input. In the training phase, the elements of \mathbf{A} and \mathbf{B} are fixed to 0, and hence BRM is simply the identity operator. In the

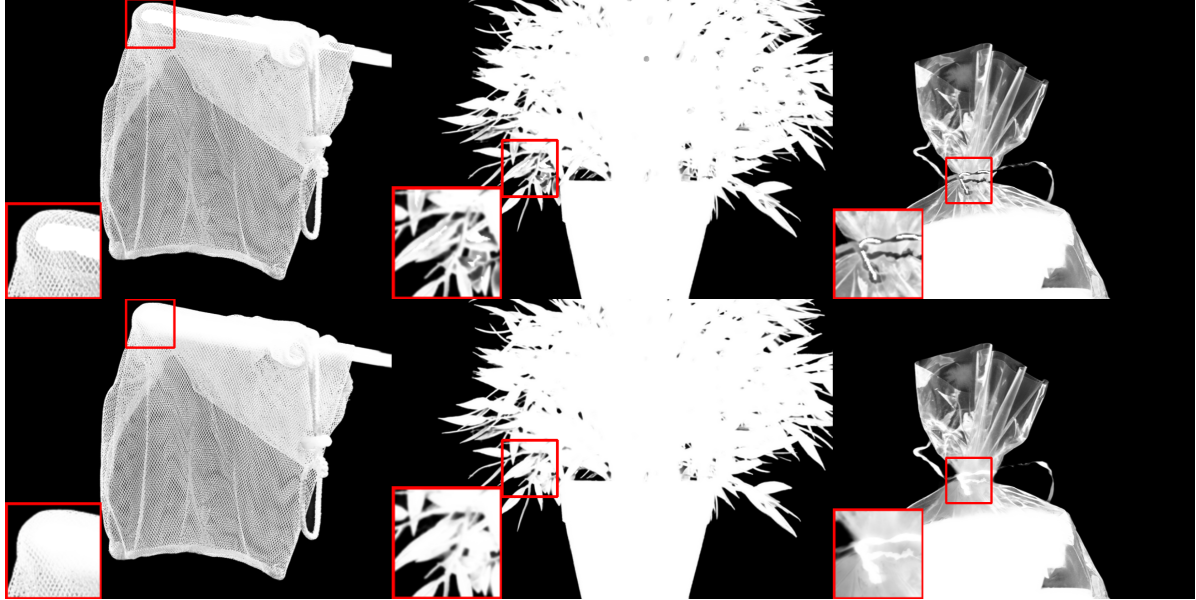


Figure 3: Illustration of the effect of BR. Figures in the first row are tested without BR. Figures in the second row are tested with BR.

inference phase, we fix all parameters of the network except for the parameters in BRM. Given a testing image, we initialize the elements of \mathbf{A} and \mathbf{B} to 0 and compute the output of the network $\hat{\alpha}_{\text{init}}$. After that, \mathbf{A} and \mathbf{B} are iteratively updated via gradient descent to minimize the cost function

$$C_1(\hat{\alpha}, \mathcal{T}) + 0.1C_2(\hat{\alpha}, \mathcal{T}), \quad (2)$$

where $\hat{\alpha}$ is the output of the network and

$$C_1(\hat{\alpha}, \mathcal{T}) = \frac{\sum_{i \in \partial\{\{i: \mathcal{T}_i=0\}} \hat{\alpha}_i^2 + \sum_{i \in \partial\{\{i: \mathcal{T}_i=1\}} (1 - \hat{\alpha}_i)^2}{\text{Card}(\partial\{i: \mathcal{T}_i=0\}) + \text{Card}(\partial\{i: \mathcal{T}_i=1\})},$$

$$C_2(\hat{\alpha}, \mathcal{T}) = \left\{ \frac{\sum_{i \in \{i: \mathcal{T}_i=0.5\}} |\hat{\alpha}_i - \hat{\alpha}_{\text{init},i}|}{\text{Card}(\{i: \mathcal{T}_i=0.5\})} \right\}^2.$$

The cost function C_1 regulates the output of the network to satisfy Assumption 2. There may be only a small number of pixels which severely violate Assumption 2. It is known that the L_2 loss is sensible to outliers. Hence in C_1 , we use the L_2 loss which automatically pay more attention to the pixels that largely violate Assumption 2. On the other hand, the cost function C_2 makes sure the output does not

largely deviate from the output of the original network. It is known that the L_1 loss is robust against a sparse set of outliers. Hence in C_2 , the squared L_1 loss ensures that the majority of pixels are not far away from the original output and meanwhile allows for a small numbers of pixels to be corrected.

Note that the BRMs are all in the decoder. Hence we only need to run the forward of the full network once and then the backward and forward computation can be restricted to the decoder. Hence the gradient descent algorithm is very efficient. In practice, we set the iteration number to be 100 with learning rate 20.

5 Experiments

In this section, we report experimental results of the proposed method. The source code is available at <https://github.com/kfeng123/LSA-Matting>.

Training data. For all experiments, the encoder of the network is pretrained on ImageNet [36], and we trained the network on the AIM training set [3] which

Sum of Absolute Differences	Troll				Doll				Donkey				Elephant				Plant				Pineapple				Plastic bag				Net																		
	overall rank	avg. small rank	avg. large rank	avg. user rank	(Strongly Transparent) Input	small	large	user	(Strongly Transparent) Input	small	large	user	(Medium Transparent) Input	small	large	user	(Medium Transparent) Input	small	large	user	(Little Transparent) Input	small	large	user	(Little Transparent) Input	small	large	user	(Highly Transparent) Input	small	large	user															
TransMatting	3.1	2.6	2.6	4	8.3	8.2	8.2	8.2	4.1	4.2	4.8	4.8	2.6	2.8	2.2	2.3	0.8	0.8	1.4	1.4	4.5	5	5	6.4	4.5	1.9	3	2.4	15.5	16.4	16.2	16.1	16.4	16.3													
TMFNet	3.5	2.5	3.1	4.9	6.1	6.1	6.5	8.3	4.2	4.5	4.5	5	2.6	2.7	2.4	2.4	0.8	0.8	1.3	1.3	4	5.2	6.6	6	1.7	1.9	2.4	14.4	14.6	14.3	17.5	18.5	21.7														
IamAlpha	4.4	5.3	4	3.9	8.4	8.4	8.4	8.3	4.4	4.6	4.4	4.4	2.7	2.7	2.7	2.7	0.9	0.9	0.9	0.9	4.8	5.2	6.2	2.3	2.5	2.8	3.1	15.8	15.8	15.8	15.9	16.5	16.5														
LPNet	4.9	4	3.8	7	7.6	8.1	3	9	4.3	4.3	5	5.7	3.1	3	9	2.8	11	0.8	0.8	1.5	1	3.9	4.2	5	3	1.7	2.1	17.6	18.10	17.9	16	16.4	16.6														
TI-MI-Net	5.1	6.4	5.9	3.1	8.3	8.7	9	9	4.4	4.7	4.6	4.3	2.8	2.9	2	2	1.1	1.1	1.3	1.4	4.7	5.2	6.2	2.2	2.3	1.9	2	15.9	16.2	15.5	16.6	19.2	18														
SiM	6	6.5	5.1	6.4	8.3	8.7	9	9	4.8	4.1	4.8	11	6	17	2.2	2	0.9	0.9	1.2	4.7	5.1	6.3	3.4	2.5	2.5	15.9	16.3	16.3	17.8	18	20.9																
PIIA Matting	9.5	6.8	11.3	10.5	9.1	10	10.13	9.3	4.3	4.6	5	5.1	2.8	3.7	16	2.7	0.9	2.3	2.1	2.7	4.7	6.8	11	8.3	11	2.7	2.7	9	4.3	17	17.2	17.3	17.5	15.5	19.1	20.7											
LSANet	10.3	9.9	10.9	10	8.4	9	7	8.8	4.5	5.7	5	6	3.3	3.5	3.1	3.1	1.9	1	1.7	1.6	5.4	7.1	19	8.5	13	2.1	2.3	10	17.3	9	17.8	16.11	16.3	17.4													
HD-Matt	11	12.4	9.6	10.9	9.5	13	10	10.7	10.7	4.7	4.8	5	5.1	2.9	3	8	2.6	1.1	1.2	1.3	5.2	5.9	6.7	7	2.4	2.8	6	3.7	1.7	17.3	10	17.6	17.1	21.5	23	20											
AdaMatting	13.2	11.8	12	15.8	10.2	11.1	18	10.8	4.9	17	5.4	5	6	6.1	2.1	2.1	0.9	0.9	1.8	1.3	4.7	6.9	9.3	21	2.6	2.6	3.7	3.9	19.2	20	19.8	22	18.7	21	20												
A2U Matting	13.4	12.1	10.5	17.6	9.3	12	9.7	10	10.9	16	4.8	13	4.9	12	5.3	10	3	12	3.1	10	2.8	10	1.2	1.9	1.9	5.1	7.8	8.5	12	2.1	18.1	17	20.6	17	20.6	12	27.3	39									
SampleNet Matting	13.7	11	13.5	16.6	9.1	10	9.7	11	9.8	11	4.3	4.8	5	5.8	3	17	3.7	17	2.8	0.9	1.1	1.1	2.1	5.1	10	6.8	24	2.5	10	4.1	3.7	12	18.6	18.9	19.3	19	19.1	24									
FGI Matting	13.8	16.6	13.1	11.5	10.3	18	10.4	15	11.7	20	4.9	19	5.3	15	5.2	9	2.5	2.7	2.2	2.4	1.2	1.2	1.2	1.3	5.6	17	6.9	12	7.8	9	2.6	2.1	3.1	6	18.9	18.9	19.3	20	28	23.28	23.62	21.7	12				
GCA Matting	15	15.8	12.8	16.6	8.8	9.5	11	11.8	4.9	16	4.8	5.8	16	3.4	16	3.7	15	3.2	16	1.1	17	1.2	1.2	1.3	5.7	18	6.9	13	7.6	8	2.8	1.5	3.1	13	4.5	20	18.3	15.9	2.5	18.5	19	20.8	20	21.7	15	24.7	28

Figure 4: Performance of the proposed method with BR on the AlaphaMatting testing set.

Sum of Absolute Differences	Troll				Doll				Donkey				Elephant				Plant				Pineapple				Plastic bag				Net						
	overall rank	avg. small rank	avg. large rank	avg. user rank	(Strongly Transparent) Input	small	large	user	(Strongly Transparent) Input	small	large	user	(Medium Transparent) Input	small	large	user	(Medium Transparent) Input	small	large	user	(Little Transparent) Input	small	large	user	(Little Transparent) Input	small	large	user	(Highly Transparent) Input	small	large	user			
TransMatting	3.1	2.6	2.6	4	8.3	8.2	8.2	8.2	4.1	4.2	4.8	4.8	2.6	2.8	2.2	2.3	0.8	0.8	1.4	1.4	4.5	5	5	6.4	4.5	1.9	3	2.4	15.5	16.4	16.2	16.1	16.4	16.3	
TMFNet	3.5	2.5	3.1	5.1	6.1	6.1	6.5	8.3	4.2	4.5	4.5	5	2.6	2.7	2.4	2.4	0.8	0.8	1.3	1.3	4	5.2	6.6	6	1.7	1.9	2.4	14.4	14.6	14.3	17.5	18	21.7		
IamAlpha	4.4	5.3	4	3.9	8.4	8.4	8.4	8.3	4.4	4.6	4.4	4.4	2.7	2.7	2.4	2.4	0.9	0.9	1.3	1.3	4.8	5.2	6.2	2.3	2.5	2.8	3.1	15.8	15.8	15.8	15.9	16.5	16.5		
LPNet	4.9	3.9	3.8	7.1	7.6	8.1	3	9	4.3	4.5	4.3	5.7	3.1	3	9	2.8	11	0.8	0.8	1.5	1	3.9	4.2	5	3	1.7	2.1	17.6	18.10	17.9	16	16.4	16.6		
TI-MI-Net	5.1	6.3	5.9	3.3	8.3	8.7	9	9	4.4	4.7	4.6	5	2.8	2.9	2	2	1.1	1.1	1.3	1.4	4.7	5.2	6.2	2.2	2.5	2.5	2.5	15.9	16.2	15.5	16.6	19.2	18		
SiM	6	6.5	5	6.5	8.3	8.7	9	9	4.8	4.1	4.8	11	6	17	2.2	2	0.9	0.9	1.3	1.4	4.7	5.1	6.3	3.4	2.5	2.5	2.5	15.9	16.4	18.8	18	20.9	8		
PIIA Matting	9.5	6.6	11.3	10.4	9.1	11	10	9.3	4.3	4.6	5	5.1	2.8	2.7	2.9	2.9	0.9	2.3	2.1	2.7	4.7	6.8	11	8.3	12	2.2	2.7	9	4.3	17	17.2	17.3	17.5	20.7	27
HD-Matt	11	12.1	9.3	11	9.5	10	10	10.7	4.7	4.9	4.8	5.1	2.9	3	8	2.6	1.1	1.2	1.3	3.6	5.2	6.7 </													

Table 2: Quantitative results on Composition-1k.

Methods	SAD	MSE	Grad	Conn
Closed-form [1]	168.1	0.091	126.9	167.9
DIM [3]	50.4	0.014	31.0	50.8
IndexNet [20]	45.8	0.013	25.9	43.7
SampleNet [5]	40.4	0.0099	-	-
Context-aware [32]	35.8	0.0082	17.3	33.2
GCA [4]	35.3	0.0091	16.9	32.5
HDMatt [7]	33.5	0.0073	14.5	29.9
A ² U [33]	32.2	0.0082	16.4	29.3
TIMI-Net [34]	29.1	0.0060	11.5	25.4
SIM [8]	28.0	0.0058	10.8	24.8
FBA [6]	26.5	0.0053	10.6	21.8
FBA + TTA [6]	25.8	0.0052	10.6	20.8
LFPNet [35]	23.6	0.0041	8.4	18.5
LFPNet + TTA [35]	22.4	0.0036	7.6	17.1
RF + CA (Ours)	25.9	0.0054	9.25	21.5
RF + CA + TTA (Ours)	24.6	0.0045	8.13	19.9

Table 3: Ablation studies on AlphaMatting training set.

Methods	SAD	MSE	Grad	Conn
Without BR	2.90	0.00540	2.47	2.45
With BR	2.87	0.00532	2.43	2.42

mizer [38] with initial learning rate $5 \cdot 10^{-5}$. We halve the learning rate every 20 epochs. The model is trained for 100 epochs with batch size 16 and weight decay 10^{-4} .

Evaluation Metrics. Following [3, 32, 32], we use the following metrics to evaluate matting methods: the sum of absolute differences (SAD), the mean square errors (MSE), the gradient errors (Grad) and the connectivity errors (Conn).

5.1 Results on Composition-1k Testing Dataset

In this section, we report evaluation results on the Composition-1k testing dataset [3] to illustrate the effectiveness of two of the proposed techniques: re-estimated foregrounds (RF), color augmentation (CA). We will evaluate the third technique in the next subsection since this technique is time-consuming in this data set. In addition, we also test our models with Test Time Augmentation (TTA). Test time augmentation was previously used by [5, 6] to fur-

ther improve the performance of the network. When TTA is used, the image is tested at three scales 0.8, 1, 1.25. For each scale, the image is rotated by $k\pi/2$, $k = 0, 1, 2, 3$ and is flipped to generate 8 images. We run the model on these $3 \times 8 = 24$ images and use the averaged outputs as the final result.

Ablation results. Table 1 lists the ablation results of the proposed three techniques. The results indicate the following phenomenons. First, while using the closed-form foreground estimation method in [1] can improve performance, the proposed re-estimated foregrounds can lead to even better results. Second, the proposed color augmentation technique can also lead to great improvement. These results confirm the effectiveness of two of the proposed techniques. Also, our results give quantitative characterization of the known facts that large input size in the training phase and TTA in the inference phase can lead to significant improvement of the performance.

Comparisons with the state-of-the-art methods. In table 2, we list the performances of some recent methods on Composition-1k data. It can be seen that for all 4 evaluation metrics, the methods of [35] are the only ones that have better performance than the proposed methods. However, the methods of [35] used extra training data beyond the AIM training set. In comparison, the proposed method is trained solely on the AIM training set. Thus, the proposed method achieves new state-of-the-art performance for all 4 measures among all methods that are solely trained on the AIM training set.

5.2 Results on AlphaMatting Dataset

In this section, we report the experimental results on AlphaMatting dataset [28]. The data distribution of AlphaMatting dataset is different from AIM dataset. To increase the generalization ability of the network, we add an additional data augmentation technique, that is, with probability 0.3, the foreground and background are blurred. Also, we train the model for 200 epochs. For all results, techniques RF, CA and TTA are used by default.

Ablation results. We evaluate the proposed backpropagating refinement (BR) technique on the AlphaMatting training set. The results, listed in Ta-

ble 3, show that BR can improve all 4 metrics. This verifies the effectiveness of the proposed BR technique.

Comparisons with the state-of-the-art methods. We evaluate the proposed method on AlphaMatting testing set. The performances of the proposed method (denoted as LSANet) and some competing methods are illustrated in Fig. 4 and Fig. 5. It can be seen that BR leads to an improvement of the ranking. While the proposed method does not rank among the top, it outperforms some recent methods, including [5, 4, 33, 7]. Also, the proposed method uses a simple architecture and is trained solely on AIM dataset. Overall, the performance of the proposed method is promising.

6 Discussion

In this paper, we investigated the use of local smoothness assumptions in deep image matting and proposed three techniques which can improve the performance of the deep image matting model significantly. We adopted a simple network and trained our model solely on AIM training data. Nevertheless, the performance of our method is promising. The application of the proposed technique to other models will be an interesting research topic.

References

- [1] Anat Levin, Dani Lischinski, and Yair Weiss, “A closed-form solution to natural image matting,” *IEEE Trans. Pattern Anal. Mach. Intell.*, vol. 30, no. 2, pp. 228–242, 2008.
- [2] Brian L. Price, Bryan S. Morse, and Scott Cohen, “Simultaneous foreground, background, and alpha estimation for image matting,” in *CVPR*, 2010, pp. 2157–2164.
- [3] Ning Xu, Brian L. Price, Scott Cohen, and Thomas S. Huang, “Deep image matting,” in *CVPR*, 2017, pp. 311–320.
- [4] Yaoyi Li and Hongtao Lu, “Natural image matting via guided contextual attention,” in *AAAI*, 2020, pp. 11450–11457.
- [5] Jingwei Tang, Yagiz Aksoy, Cengiz Öztireli, Markus H. Gross, and Tunç Ozan Aydin, “Learning-based sampling for natural image matting,” in *CVPR*, 2019, pp. 3055–3063.
- [6] Marco Forte and François Fleuret, “ F , B , alpha matting,” *arXiv: 2003.07711*, 2020.
- [7] Haichao Yu, Ning Xu, Zilong Huang, Yuqian Zhou, and Humphrey Shi, “High-resolution deep image matting,” in *AAAI*, 2021, pp. 3217–3224.
- [8] Yanan Sun, Chi-Keung Tang, and Yu-Wing Tai, “Semantic image matting,” in *CVPR*, 2021, pp. 11120–11129.
- [9] Yung-Yu Chuang, Brian Curless, David Salesin, and Richard Szeliski, “A bayesian approach to digital matting,” in *CVPR*, 2001, pp. 264–271.
- [10] Jue Wang and Michael F. Cohen, “Optimized color sampling for robust matting,” in *CVPR*, 2007.
- [11] Eduardo S. L. Gastal and Manuel M. Oliveira, “Shared sampling for real-time alpha matting,” *Computer Graphics Forum*, vol. 29, no. 2, pp. 575–584, may 2010.
- [12] Kaiming He, Christoph Rhemann, Carsten Rother, Xiaoou Tang, and Jian Sun, “A global sampling method for alpha matting,” in *CVPR*, 2011, pp. 2049–2056.
- [13] Ehsan Shahrian, Deepu Rajan, Brian L. Price, and Scott Cohen, “Improving image matting using comprehensive sampling sets,” in *CVPR*, 2013, pp. 636–643.
- [14] Xiaoxue Feng, Xiaohui Liang, and Zili Zhang, “A cluster sampling method for image matting via sparse coding,” in *ECCV*, 2016, pp. 204–219.
- [15] Jian Sun, Jiaya Jia, Chi-Keung Tang, and Heung-Yeung Shum, “Poisson matting,” *ACM Trans. Graph.*, vol. 23, no. 3, pp. 315–321, 2004.
- [16] Qifeng Chen, Dingzeyu Li, and Chi-Keung Tang, “KNN matting,” *IEEE Trans. Pattern Anal. Mach. Intell.*, vol. 35, no. 9, pp. 2175–2188, 2013.
- [17] Yagiz Aksoy, Tunç Ozan Aydin, and Marc Pollefeys, “Designing effective inter-pixel information flow for natural image matting,” *CVPR*, pp. 228–236, 2017.
- [18] Donghyeon Cho, Yu-Wing Tai, and In-So Kweon, “Natural image matting using deep con-

volutional neural networks,” in *ECCV*, 2016, vol. 9906, pp. 626–643.

[19] Sebastian Lutz, Konstantinos Amplianitis, and Aljosa Smolic, “Alphagan: Generative adversarial networks for natural image matting,” in *BMVC*, 2018, p. 259.

[20] Hao Lu, Yutong Dai, Chunhua Shen, and Songcen Xu, “Indices matter: Learning to index for deep image matting,” in *ICCV*, 2019, pp. 3265–3274.

[21] Shaofan Cai, Xiaoshuai Zhang, Haoqiang Fan, Haibin Huang, Jiangyu Liu, Jiaming Liu, Jiaying Liu, Jue Wang, and Jian Sun, “Disentangled image matting,” in *ICCV*, 2019, pp. 8818–8827.

[22] Soumyadip Sengupta, Vivek Jayaram, Brian Curless, Steven M. Seitz, and Ira Kemelmacher-Shlizerman, “Background matting: The world is your green screen,” in *CVPR*, 2020, pp. 2288–2297.

[23] Yu Qiao, Yuhao Liu, Xin Yang, Dongsheng Zhou, Mingliang Xu, Qiang Zhang, and Xiaopeng Wei, “Attention-guided hierarchical structure aggregation for image matting,” in *CVPR*, 2020, pp. 13673–13682.

[24] Tong He, Zhi Zhang, Hang Zhang, Zhongyue Zhang, Junyuan Xie, and Mu Li, “Bag of tricks for image classification with convolutional neural networks,” in *CVPR*, 2019, pp. 558–567.

[25] Kaiming He, Xiangyu Zhang, Shaoqing Ren, and Jian Sun, “Deep residual learning for image recognition,” in *CVPR*, 2016, pp. 770–778.

[26] Jie Hu, Li Shen, Samuel Albanie, Gang Sun, and Enhua Wu, “Squeeze-and-excitation networks,” *IEEE Trans. Pattern Anal. Mach. Intell.*, vol. 42, no. 8, pp. 2011–2023, 2020.

[27] Youngwan Lee, Joong-Won Hwang, Sangrok Lee, Yuseok Bae, and Jongyoul Park, “An energy and gpu-computation efficient backbone network for real-time object detection,” in *CVPRW*, 2019, pp. 752–760.

[28] Christoph Rhemann, Carsten Rother, Jue Wang, Margrit Gelautz, Pushmeet Kohli, and Pamela Rott, “A perceptually motivated online benchmark for image matting,” in *CVPR*, 2009, pp. 1826–1833.

[29] Thomas Germer, Tobias Uelwer, Stefan Conrad, and Stefan Harmeling, “Fast multi-level foreground estimation,” in *ICPR*, 2020, pp. 1104–1111.

[30] Won-Dong Jang and Chang-Su Kim, “Interactive image segmentation via backpropagating refinement scheme,” in *CVPR*, 2019, pp. 5297–5306.

[31] Konstantin Sofiuk, Ilia A. Petrov, Olga Barianova, and Anton Konushin, “F-BRS: rethinking backpropagating refinement for interactive segmentation,” in *CVPR*, 2020, pp. 8620–8629.

[32] Qiqi Hou and Feng Liu, “Context-aware image matting for simultaneous foreground and alpha estimation,” in *ICCV*, 2019, pp. 4129–4138.

[33] Yutong Dai, Hao Lu, and Chunhua Shen, “Learning affinity-aware upsampling for deep image matting,” in *CVPR*, 2021, pp. 6841–6850.

[34] Yuhao Liu, Jiake Xie, Xiao Shi, Yu Qiao, Yujie Huang, Yong Tang, and Xin Yang, “Tripartite information mining and integration for image matting,” in *ICCV*, 2021, pp. 7555–7564.

[35] Qinglin Liu, Haozhe Xie, Shengping Zhang, Bineng Zhong, and Rongrong Ji, “Long-range feature propagating for natural image matting,” in *ACM Multimedia*, 2021, pp. 526–534.

[36] Jia Deng, Wei Dong, Richard Socher, Li-Jia Li, Kai Li, and Fei-Fei Li, “Imagenet: A large-scale hierarchical image database,” in *CVPR*, 2009, pp. 248–255.

[37] Tsung-Yi Lin, Michael Maire, Serge J. Belongie, James Hays, Pietro Perona, Deva Ramanan, Piotr Dollár, and C. Lawrence Zitnick, “Microsoft COCO: common objects in context,” in *ECCV*, 2014, pp. 740–755.

[38] Diederik P. Kingma and Jimmy Ba, “Adam: A method for stochastic optimization,” in *ICLR*, 2015.